THE AMERICAN SOCIETY OF MECHANICAL ENGINEERS
345 E. 47 St., New York, N.Y. 10017

86-GT-246

Horseshoe Vortex Formation Around a Cylinder

W. A. ECKERLE
United Technologies Research Center
East Hartford, CT 06108

L. S. LANGSTON
Department of Mechanical Engineering
University of Connecticut
Storrs, CT 06268

ABSTRACT

An experimental investigation was conducted to characterize a symmetrical horseshoe vortex system in front of and around a single large-diameter right cylinder centered between the sidewalls of a wind tunnel. Surface flow visualization and surface static pressure measurements as well as extensive mean velocity and pressure measurements in and around the vortex system were acquired. The results lend new insight into the formation and development of the vortex system. Contrary to what has been assumed previously, a strong vortex was not identified in the streamwise plane of symmetry, but started a significant angular distance away from it. Rather than the multiple vortex sytems reported by others, only a single primary vortex and saddle point were found. The scale of the separation process at the saddle point was much smaller than the scale of the approaching boundary layer thickness. Results of the present study not only shed light on such phenomena as the nonsymmetrical endwall flow in axial turbomachinery but can also be used as a test case for three-dimensional computational fluid mechanics computer codes.

NOMENCLATURE

C_f	Skin friction coefficient
Cp_s	Static pressure coefficient, $(P_s-Ps_o)/q_o$
Cp_T	Loss coefficient, $(P_{To}-P_T)/q_o$
$\overline{Cp}_T$	Mass - averaged loss coefficient, eqn. (2)
D	Cylinder diameter, 29.85 cm
H	Boundary - layer shape factor, δ^*/θ
MS	Test-section midspan plane
n	Exponent in power-law profile representation, $2/(H-1)$
P_s	Local static pressure
P_{so}	Reference static pressure near test-section entrance
P_T	Local total pressure
P_{To}	Reference total pressure near test-section entrance
Q	Local velocity magnitude
q_o	Dynamic pressure near test-section entrance
R	Radial distance from center of cylinder, Fig. 1
Re	Reynolds number based on boundary-layer momentum thickness
U_o	Reference velocity near the test-section entrance
x,y,z,	Orthogonal coordinate system as defined in Fig. 1
z_o	Lower limit of mass-averaged loss integral, either 0 or D/2
z_w	Distance from test-section plane of symmetry to sidewall, 0.91m
β	Position angle relative to plane of symmetry, Fig. 1
δ	Boundary-layer thickness
δ^*	Boundary-layer displacement thickness
θ	Boundary-layer momentum thickness
ρ	Density
μ	Viscosity
ν	Kinematic viscosity, μ/ρ

INTRODUCTION

The three-dimensional separation of a boundary layer approaching a bluff body, an airfoil, or a cascade of airfoils mounted on a wall is a commonplace phenomenon in fluid mechanics. The separation commences at a wall saddle point of separation, downstream of which a vortex system is formed in front of and around the body. This system, made up of the boundary layer and some portion of the mainstream flow, is generally referred to as a horseshoe vortex (or vortices) in the (English) literature.

The symmetrical separation of boundary layer flow normal to a single cylinder (or a cascade of cylinders) is perhaps the simplest of geometries that demonstrate the horseshoe vortex phenomenon (e.g., Ref. 1), while the vortex system formed on the endwall of a cascade of turbine airfoils (e.g. Ref. 2) might be considered to be one of the most complex of the family of such flows.

Presented at the International Gas Turbine Conference and Exhibit
Dusseldorf, West Germany—June 8-12, 1986

This paper deals with the experimental study of the simple cylinder vortex system. Aerodynamic measurements were made to define the horseshoe vortex system formed around a single cylinder mounted between endwalls in a wind tunnel. Because of the existance of the sidewalls of the tunnel, the cylinder model approximates one element of a cascade of cylinders. The tests were carried out at a relatively high Reynolds number with turbulent boundary layers on the endwalls. The objectives of the study were as follows:

1. There have been a number of studies carried out to measure and explain cylinder endwall flow and these have been reviewed by Eckerle[1]. The conclusion of this review is that few or no measurements have been taken in the vortex region itself, especially in the region of vortex formation. Also, in most studies, the scale of the experiment was too small for accurate and detailed measurements. In the study presented here, measurements were made in the vortex region, and the cylinder model scale was about 100 times larger than the pressure probe scale.
2. Often it is possible to study and understand a simple member of a fluid flow family to explain and predict the behavior of a more complex member of that family. The study here represents the flow into a cascade of cylinders with zero angle of attack (no lift), at a Reynolds number based on cylinder diameter representative of many turbomachinery applications and with a large scale that would be difficult to achieve in an airfoil cascade. One objective then is to shed more light on the important problem of endwall flows in turbine cascades.
3. The measurments were taken in such a way (i.e., inlet and exit conditions to a control volume with interior flow measurements) that they can be used as a test case for three-dimensional computational fluid mechanics computer codes.

The emphasis of this paper is to elucidate details of the horseshoe vortex structure and to indicate significant differences between the measured vortex characteristics and the vortex structure that has been assumed by others. A more detailed discussion of the results, e.g., pressure distribution on the cylinder surface is contained in Ref. [1].

EXPERIMENTAL APPARATUS

Testing was conducted in the University of Connecticut Low Speed Wind Tunnel. Details of this tunnel and specific modifications for this experiment are contained in Ref. 1. The test-section lower endwall was constructed to facilitate acquisition of static pressures during this program. The lower endwall contained a rotatable disk to which a 29.8-cm diameter cylinder that spanned the test section was concentrically mounted. Both the lower endwall and cylinder contained four rows of static pressure taps. The radial position of the taps on the endwall and the vertical positon of the taps on the cylinder were staggered so that dense static pressure distributions at any desired angular location on both the endwall and cylinder surfaces could be obtained by sequentially rotating each row of taps to a desired angular location. Accurate and repeatable angular positioning of the disk was achieved with indexing holes machined near the disk's outer edge.

A schematic of the test section along with the coordinate systems used in this effort are shown in Fig. 1. The origin of the coordinate systems coincides with the cylinder and disk center on the lower endwall. Angular and radial positions are

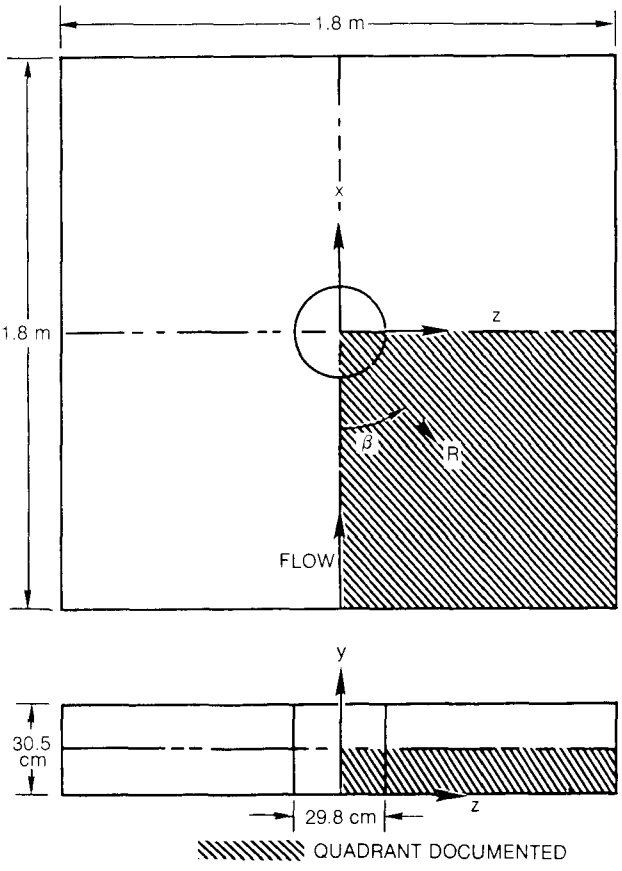

FIG. 1 SCHEMATIC SHOWING TEST SECTION WITH CYLINDER AND COORDINATE SYSTEMS

denoted by β and R, respectively. Cartesian coordinates representing streamwise, vertical, and transverse locations are x, y, and z, respectively. The experiment was designed to create vertical and horizontal planes of symmetry at the test-section centerline and midheight, respectively. As shown in Fig. 1, the lower quadrant on the right side of the test-section, when viewed facing downstream, was chosen for documentation.

Interior fluid measurements were obtained with a five-hole combination probe manufactured by United Sensor Co., (Model No. DC-0.093-24-F). Probe calibrations, which were checked several times during testing, provided local total pressure, static pressure, and velocity magnitude and direction for a range in pitch angle of $\pm$ 30 deg. The probe tip diameter, which was aligned with the shaft axis so that the tip rotated but did not translate as the probe was rotated about its shaft axis, was 2.4 mm. This tip diameter was less than one percent of the cylinder diameter and span. Excellent agreement was observed between probe static pressures measured near the bottom endwall and corresponding endwall pressures measured without the probe in the vicinity of the static tap. The probe was positioned vertically and in yaw with a calibrated probe drive that was mounted to a mechanized positioner located on the top endwall. Precise angular (β) and radial (R) probe positions were determined by aligning the probe tip with an endwall static tap that was positioned at the desired measurement location. Estimated experimental uncertainties associated with the five-hole probe measurements and position are:

Angular position,	± 0.2 deg
Yaw angle	± 0.5 deg
Cp_T	± 0.0062
Cp_s	± 0.0085
$\frac{Q}{U_o}$	± 0.0085
Pitch angle	± 0.15 deg
Vertical position, y	± 0.05 cm
Radial position, R	± 0.04 cm

Odds are 20 to 1 that the measured values were within the uncertainty intervals listed above.

Velocity profile data for the boundary layer near the test-section entrance were obtained with pitot-static probes. Flow visualization patterns on the endwall and cylinder surfaces were obtained using the ink/oil of wintergreen technique of Langston and Boyle [3].

TEST CONDITIONS

All testing for this study was conducted with a velocity at the test-section entrance of 30.5 m/sec corresponding to a Reynolds number based on cylinder diameter of 5.5×10^5. Velocity profile data for the approaching boundary layer were acquired near the test-section entrance at $x/D = -2.72$ with the cylinder installed. The following table lists the measured boundary-layer dimensions and properties at the test-section centerline.

TABLE I

TEST-SECTION CENTERLINE ENTRANCE
BOUNDARY-LAYER PARAMETERS WITH CYLINDER INSTALLED

$x/D = -2.72$

z/D	δ/D	δ^*/D	θ/D	δ^*/θ	C_f	Re_θ
0	0.099	0.0154	0.0114	1.35	0.0028	6149

The test section inlet, carefully constructed of porous plates, honeycomb, and fine mesh screen, created a uniform entrance flow field to within ± 2 percent of the above values. The streamwise turbulence intensity of the core flow was less than one percent.

EXPERIMENTAL RESULTS

Endwall surface static pressures are presented along with interior fluid measurements obtained with a five-hole probe. The vortex characteristics deduced from these measurements are then integrated with surface flow visualizations to characterize the vortex formation process.

Endwall Static Pressure Measurements

Static pressure distributions are presented in coefficient form using the polar coordinate system defined in Fig. 1. The pressure distribution in the plane of symmetry, $\beta = 0$, is presented in Fig. 2. Radial locations are normalized by the cylinder diameter, and the abscissa corresponds to the cylinder leading edge. Upstream of the separation region, the distribution displays a characteristic rise in pressure due to the blockage of the cylinder. Unlike the potential-flow distribution shown by the solid line, the experimental distribution begins to decrease a short distance downstream of the saddle point determined from the endwall flow visualizations. The distribution displays a local minimum approximately two tenths of a cylinder diameter from the cylinder leading edge, then increases rapidly from that point to a value of one at the endwall-cylinder junction. The coefficient value of one indicates that loss-free core flow stagnated at the junction. Location of the saddle point in an adverse pressure gradient, not at the local peak pressure, is consistent with the work of Langston and Wagner [4]. They applied Oswatitch's model [5] to saddle-point behavior and predict that the saddle point occurs in an adverse pressure gradient.

The difference between experimental and potential-flow values upstream of the saddle point is the result of the mean flow accelerating through the test section due to the increasing boundary layers on the uncontoured endwalls. The experimental values in Fig. 2 that correspond with five-hole probe traverses were corrected for the effect of the thickening boundary layer. The corrected values are close to the potential-flow values.

The experimental distribution in Fig. 2 is plotted with the limited results of Ram [6] and East and Hoxey [7]. These experiments were conducted in large wind tunnels so that corrections for thickening boundary layers are insignificant. Static pressures measured upstream of the saddle point are close to the corrected values from this experiment, although Ram's data are slightly higher than the other two sets. Ram's results in the separation zone exhibit the same trend as data from this experiment.

Potential-flow and measured endwall static pressure contours throughout the documented quadrant are shown in Fig. 3. The potential-flow results are for a cascade of cylinders spaced to simulate the test-section sidewalls. Comparing these two figures, the pressure distributions are, as expected, quite similar outside of the separation region. Inside the separation region, the experimental contours display a large dip near $R/D = 0.72$. This dip, which was observed in the plane of symmetry data, persists around the cylinder up to approximately $\beta = 60$ deg. Beyond this angular plane, the dip is no longer present, and the experimental contours are shaped more like that of the potiential-flow contours. This

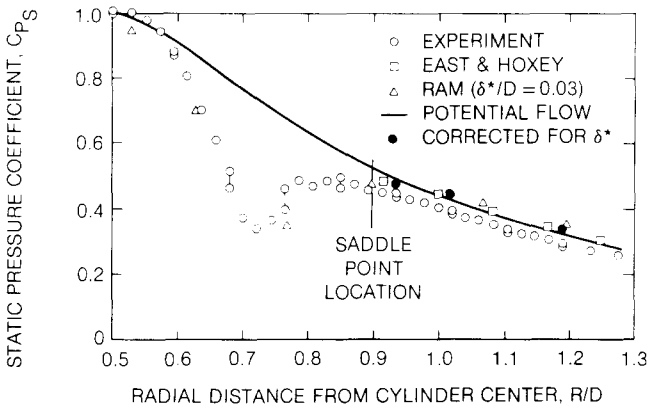

FIG. 2 COMPARISON OF PLANE OF SYMMETRY STATIC PRESSURE DISTRIBUTIONS

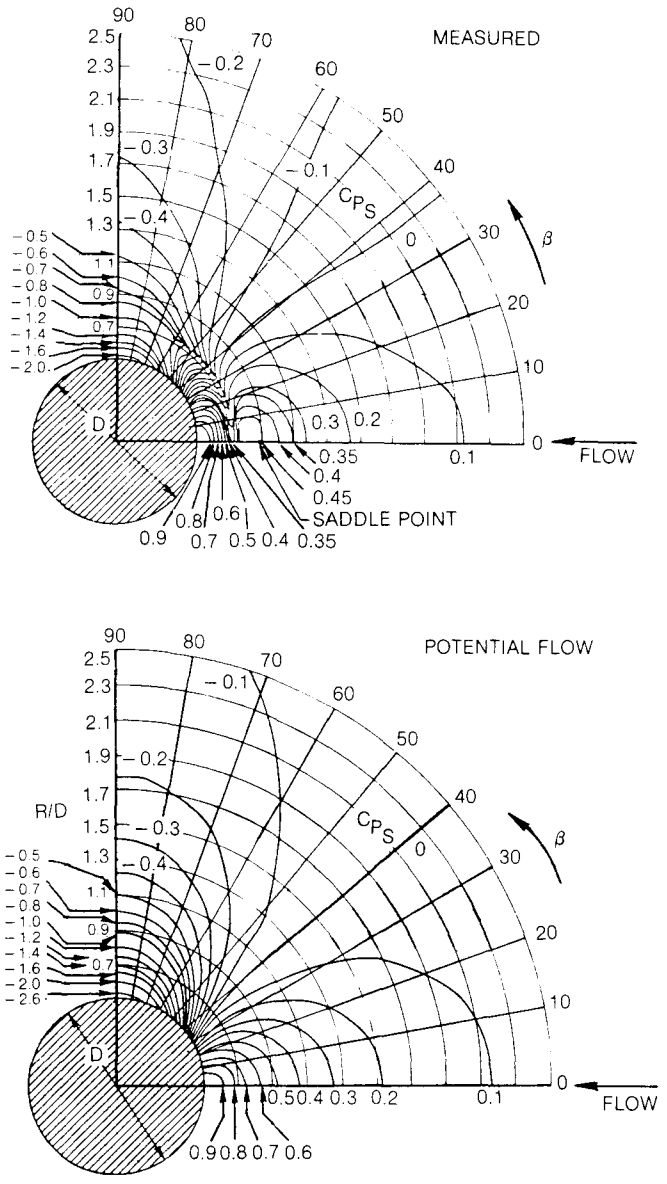

FIG. 3 COMPARISON OF MEASURED ENDWALL PRESSURE DISTRIBUTION WITH POTENTIAL-FLOW PRESSURE DISTRIBUTION

similarity indicates that the strong pressure field associated with the mean flow acceleration around the cylinder, which is represented by the potential-flow solution, negated the local pressure minimum created in the separation region.

Five-Hole Probe Measurements

Data were acquired with a five-hole probe in the angular planes defined by β = -5, 0, 5, 25, 45, and 90 deg. The probe was traversed at 81 radial locations to define the flow field adjacent to and inside of the separation region. Data were recorded from y/D ≅ 0.0085 to the test-section midspan. This smaller value, approximately one probe tip diameter from the endwall, represents the lowest point for which data could be acquired without endwall interference. This determination was primarily based on endwall static pressure data acquired in this test program with and without the probe in proximity of a static pressure tap. Data obtained up to 0.2 cylinder diameters from the endwall are discussed. The data in the region between y/D = 0.2 and the test-section midspan (y/D = 0.511) do not substantially vary from the midspan values. The endwall-region data are presented in the form of in-plane velocity vectors, static pressure contours, and total pressure contours.

The radial velocity components for the angular planes given by β = 0, 25, and 90 deg are presented. The data are displayed as vectors centered at the measurement point. The in-plane pitch angles are based on the in-plane components, not on the total velocity measured with the five-hole probe. The vectors are normalized by the reference velocity measured at the test-section entrance. The ordinate and abscissa in the figures represent the cylinder O.D. and endwall, respectively.

The plane of symmetry velocity vectors are shown in Fig. 4. Upstream of the endwall saddle point, the vectors take on the appearance of a two-dimensional boundary layer, though vortex stretching is present. The outer edge of the approaching boundary layer at R/D = 0.94 is at y/D ≅ 0.13. The separation streamline between forward and reverse flow is very shallow. A straight line drawn from the saddle point to the streamline location at R/D = 0.766 represents a separation angle of approximately four degrees. The shallowness of this line is markedly different from the multiple vortex models developed in the literature, e.g., that of Baker [8]. Following the flow field from the saddle point toward the cylinder, the velocity vectors indicate that flow in the boundary layer and outside of the boundary layer pitched downward, rotated 180 degress, and proceeded toward the saddle point. Blank areas are present in the traverses nearest the cylinder because the flow pitch angle was out of the probe calibration range. Data were acquired in these regions, however, to qualitatively determine the flow direction.

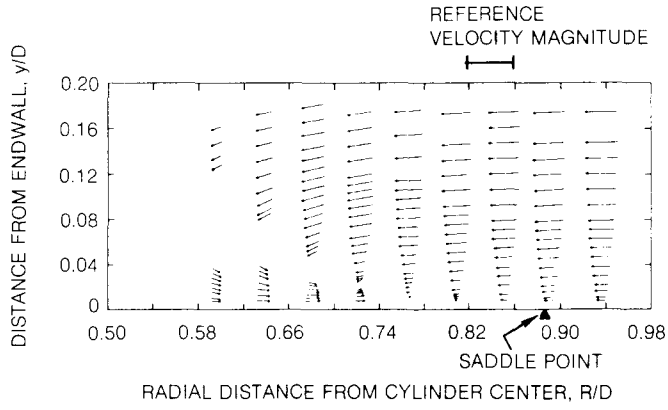

FIG. 4 VELOCITY VECTORS IN THE PLANE OF SYMMETRY

The plane of symmetry flow pattern deduced from the five-hole probe data and surface static pressure data is sketched in Fig. 5. Loss-free fluid outside the boundary layer stagnated at the endwall-cylinder junction. Five-hole probe measurements at R/D = 0.598 contain negative pitch angles up to y/D ≅ 0.3 indicating that flow from approximately two approaching boundary-layer thicknesses away from the endwall entered the juncture region. The reverse flow accelerated as it moved away from the endwall-cylinder juncture in order to accomodate the incoming flow, which separated at a shallow angle. The favorable endwall static pressure gradient is consistent with this pattern. At approximately R/D = 0.72, the

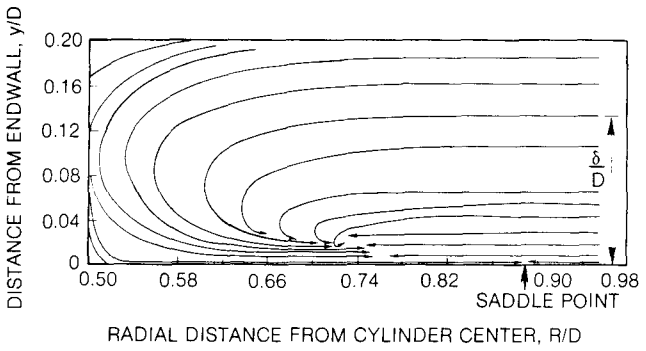

FIG. 5 FLOW PATTERN IN THE PLANE OF SYMMETRY

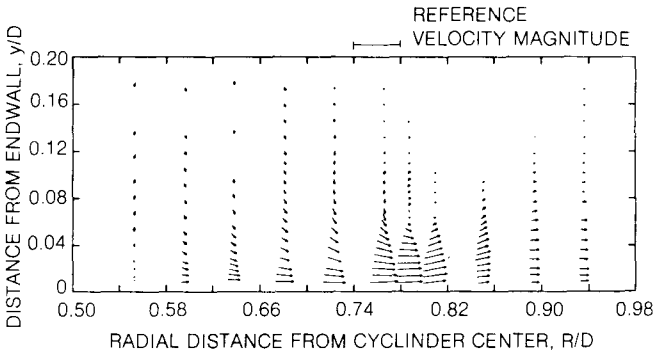

FIG. 7 VELOCITY VECTORS IN THE 90-DEG PLANE

reverse flow started stagnating with the incoming flow. The abrupt reverse flow deceleration caused by the blockage is indicated by the strong endwall adverse pressure gradient in this region. The reverse flow did not roll up to form a vortex, however. The vectors clearly show that a closed vortex was not present in the plane of symmetry, though positive pitch angles in a portion of the reverse flow at R/D = 0.72 and y/D = 0.02 may indicate the start of vortex formation. Rather than rolling up, the reverse flow passed out the plane and proceeded tangentially around the cylinder next to the separation line. Note that the reverse flow was confined to the lower 15 percent of the boundary layer as it passed out of the plane.

Velocity vectors in the 5-deg plane show a flow pattern similar to that shown in the plane of symmetry. Velocity vectors for the 25-deg plane, however, show a well-formed vortex (Fig. 6). The vortex, then, became fully formed between the plane of symmetry and 25-deg plane. The vortex center in the 25-deg plane was at R/D = 0.71 and y/D = 0.035. This was approximately one third of the incoming boundary-layer thickness from the endwall. The vortex itself was confined to a region that extended less than one boundary-layer thickness from the endwall. The radial location of the vortex center is close to that of the local static pressure minimum on the endwall in this plane.

The velocity vectors in the 45-deg plane are similar to these presented for the 25-deg plane. Between the 25-deg and 45-deg planes, however, the vortex center moved radially outward to R/D = 0.735. The vortex structure in the 90-deg plane was much weaker than that in the 45-plane. The velocity vectors in Fig. 7 faintly show a vortex center at R/D = 0.80 and y/D = 0.07. The vortex was not symmetric with the secondary flow near the endwall stronger than that on the core-flow side of the vortex. The reduced

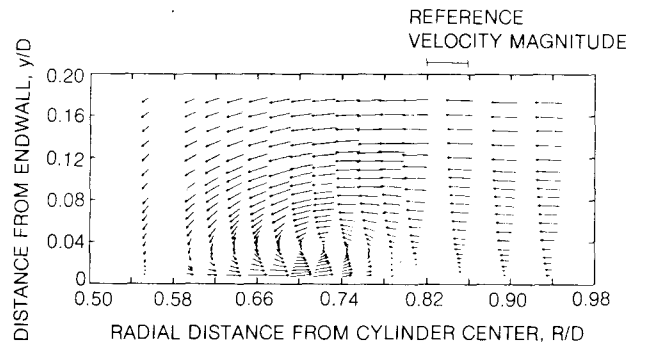

FIG. 6 VELOCITY VECTORS IN THE 25-DEG PLANE

vortex strength, which was also indicated by the endwall static pressure distribution, can be attributed to the streamwise acceleration of the mean flow around the cylinder.

Static pressure coefficient contours corresponding to the velocity vector plots are shown in Figs. 8-10. Upstream of the endwall saddle point, the static pressure contours in the plane of symmetry are nearly vertical except near the endwall surface. The pressures adjacent to the endwall were larger than those measured in the core flow. This trend can also be seen in the comparison between potential-flow and corrected endwall static pressures in the plane of symmetry (Fig. 2). The assumption of constant static pressure through the two-dimensional boundary layer at a given streamwise location upstream of the saddle point is inaccurate. The cylinder created a stronger adverse pressure gradient in the viscous sublayer.

The pressure distribution closer to the cylinder was significantly skewed by the recirculating flow. A local pressure minimum at y/D $\cong$ 0.04 and R/D $\cong$ 0.73 is marked by the closed contours. The velocity vectors show that this small minimum is not associated with a vortex. The minimum pressure in the plane was adjacent to the endwall at the same radial location. This minimum is associated with the reverse flow first accelerating away from the cylinder and then decelerating when blocked by the streamwise flow. The coefficients near the cylinder are close to one. They indicate that low-loss fluid from outside the boundary layer passed next to the cylinder at a low velocity prior to stagnating at the endwall cylinder junction.

The contours in the 25-deg plane, Fig. 9, clearly correspond to the well-formed vortex structure shown in the corresponding velocity vector plot. The center of the closed pressure contours corresponds with the vortex center indicated by the velocity vectors. The static pressure coefficient at the vortex center is 40 percent of the test-section entrance dynamic head below the test-section midspan coefficient measured at the same radial position. The pressure contours indicate that the pressure distribution upstream of the separation line was also substantially altered by the vortex structure.

In the 90-deg plane, where the vortex strength was significantly reduced, pressure profiles in Fig. 10 show that pressure at the vortex core was only slightly less than surrounding pressure. The contours tend to be vertical and increase in value radially outward. The pressure field associated with the two-dimensional acceleration of the flow around the cylinder was clearly dominant. The vortex had only a small local effect on the pressure distribution.

Total pressure data from the five-hole probe measurements have been expressed as loss coefficients:

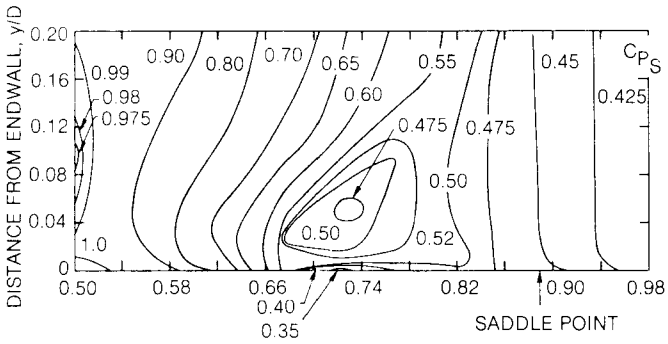

FIG. 8 STATIC PRESSURE CONTOURS IN PLANE OF SYMMETRY

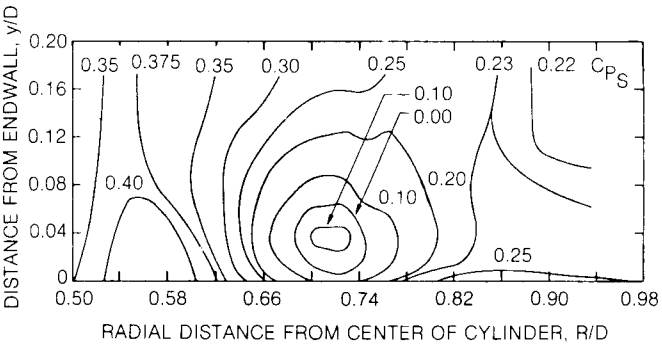

FIG. 9 STATIC PRESSURE CONTOURS IN 25-DEG PLANE

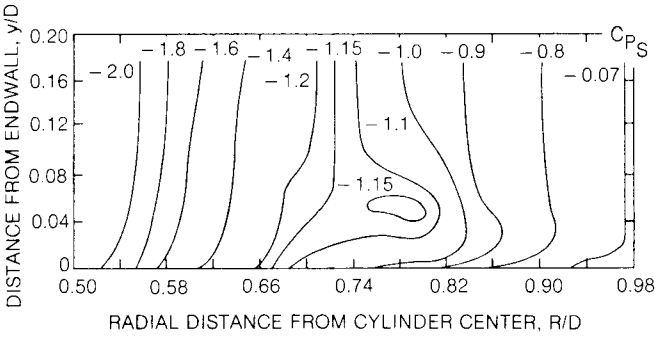

FIG. 10 STATIC PRESSURE CONTOURS IN 90-DEG PLANE

$$C_{P_T} = \frac{P_{T_o} - P_T}{q_o} \qquad (1)$$

where the test-section entrance conditions are again used for references. The loss contours for the same three planes are shown in Fig. 11. Upstream of the saddle point, the contours are nearly horizontal, like an attached two-dimensional boundary layer. The edge of the boundary layer approaching the saddle point was at y/D = 0.13. Downstream of the saddle point, the low-loss contour bends around and touches the abscissa at R/D = 0.54. This pattern shows the radial extent of the low-loss fluid in front of the cylinder. The contours also show the high total pressure loss associated with this low-loss fluid accelerating away from the endwall-cylinder junction. The region of highest loss, C_{P_T} = 0.6, occurred at R/D = 0.74, where the reverse flow next to the endwall interacted with the streamwise flow. The loss contours in the 25-deg plane show high losses at the location corresponding to the vortex center. The losses at the vortex center were 80 percent of the entrance dynamic pressure. Though these losses associated with the rollup were high, they were localized. The region of low losses adjacent to the cylinder location is larger than the same region in the plane of symmetry. For the 90-deg plane, the contours indicate that the high-loss region is displaced to the same location as the vortex center. The high-loss fluid created during the rollup process, then, simply accumulated at the vortex center and passed around the cylinder with the vortex. The magnitude of the losses in the vortex did not increase during the passage from the 25-deg to the 90-deg plane. The size of the low-loss fluid region adjacent to the cylinder increased only a small amount from that same region in the 25-deg plane.

The mass-averaged pressure loss at any streamwise plane in the test section is given by:

$$\overline{C_{P_T}} = \frac{\int_{z_o}^{z_w} \int_{o}^{MS} C_{P_T} \, u \, dy \, dz}{\int_{z_o}^{z_w} \int_{o}^{MS} u \, dy \, dz} \qquad (2)$$

The limits in Eq. (2) reflect the two planes of symmetry. The sidewall boundary layers were not measured and are not included in the loss calculation. The losses calculated across the entrance plane are quite uniform at four percent of the reference dynamic

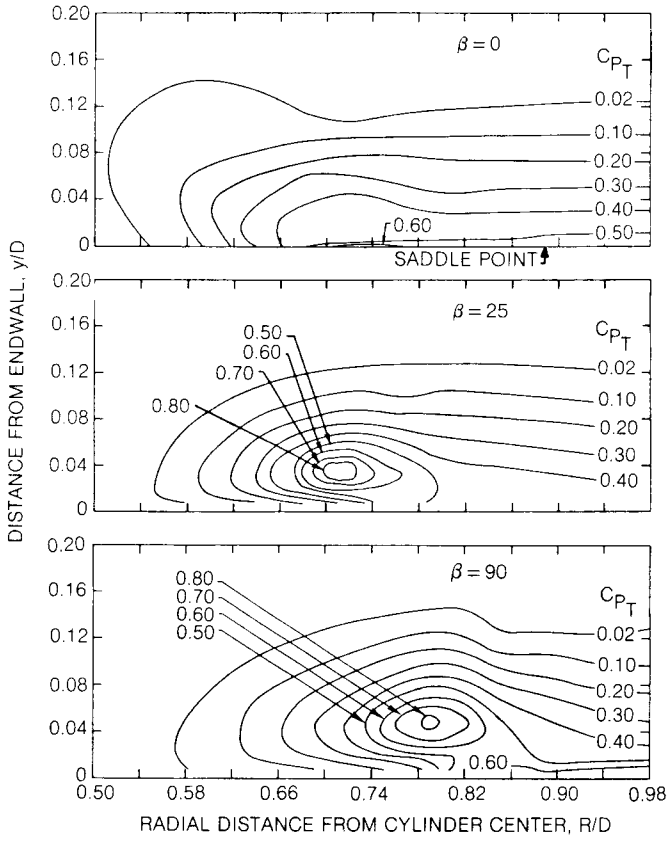

FIG. 11 TOTAL PRESSURE LOSS

pressure. The loss distribution for the 90-deg plane is in Fig. 12. Each point represents the mass-averaged loss of a particular traverse. The 90-deg plane losses are nonuniform. Adjacent to the cylinder, the losses are quite low since low-loss fluid from the core flow occupied this region. Relatively high losses at z/D = 0.8 are associated with high loss fluid that accumulated in the vortex core during the rollup process. Farther away from the cylinder, z/D > 1.15, losses level out at around five percent of the reference dynamic pressure.

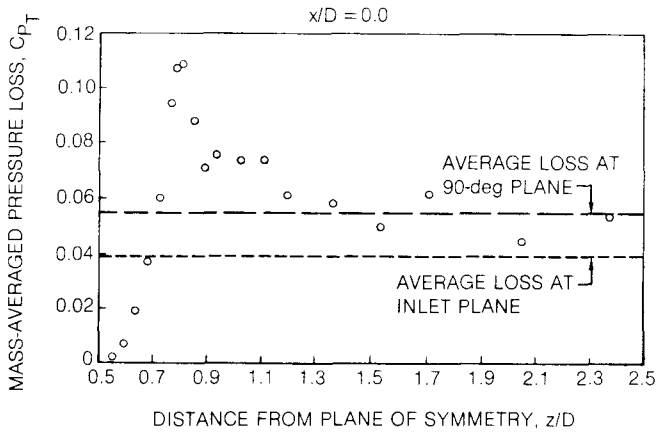

FIG. 12 PRESSURE LOSS DISTRIBUTION IN THE 90-DEG PLANE

A check on the integration procedure for calculating the above losses was accomplished by comparing the calculated mass flow through each of the planes (the denominator in Eq. (2)). Mass flow through the 90-deg plane was 3.4 percent above that in the entrance plane. This agreement indicates that the above integration procedure provided accurate values for $\overline{C}_{P_T}$.

A comparison for the above loss calculations is the loss for an equivalent turbulent boundary layer developing on a flat plate without a cylinder. Substituting the power-law formulation for the velocity distribution into Eq. (2) yields:

$$\overline{C_{P_T}} = \frac{\frac{n}{n+1} - \frac{n}{n+3}}{\frac{n}{n+1}\left(\frac{MS}{\delta}\right)^{\frac{n+1}{n}}} \qquad (3)$$

The calculated loss coefficient at the test-section entrance centerline, using measured boundary-layer parameters, is $\overline{C}_{P_T} = 0.038$. This value is very close to the 0.039 value calculated by integrating experimental data. In the absence of a pressure gradient, Schlichting [9] gives the following expression for the boundary-layer thickness as a function of streamwise distance:

$$\delta(x) = 0.37 \times \left(\frac{Ux}{\nu}\right)^{-1/5} \qquad (4)$$

Equation (4) was used to estimate the flat-plate boundary-layer development of a flow starting with the test-section entrance conditions. The boundary-layer thickness was calculated for a length equal to x/D = 2.72 (the distance to the 90-deg plane). The calculated value of was substituted into Eq. (3), resulting in a loss coefficient of 0.054. This value is identical to the measured loss in the 90-deg plane. It is concluded, then, that the overall loss associated with the horseshoe vortex formation is small. Losses associated with the vortex rollup are offset by low losses adjacent to the cylinder. Langston, et. al. [2] found the same trend in their cascade experiment. The measured losses in the initial portion of the cascade were only slightly larger than those measured upstream of the saddle point. Significant losses, measured farther downstream in the passage, were associated with the interaction of the passage vortex with the airfoil suction surface in the region of uncovered turning.

Flow Visualization

A photograph of the endwall streaklines along with an accompanying flow diagram are contained in Fig. 13. Two singular points, a saddle point and an attachment point, can be seen in the plane of

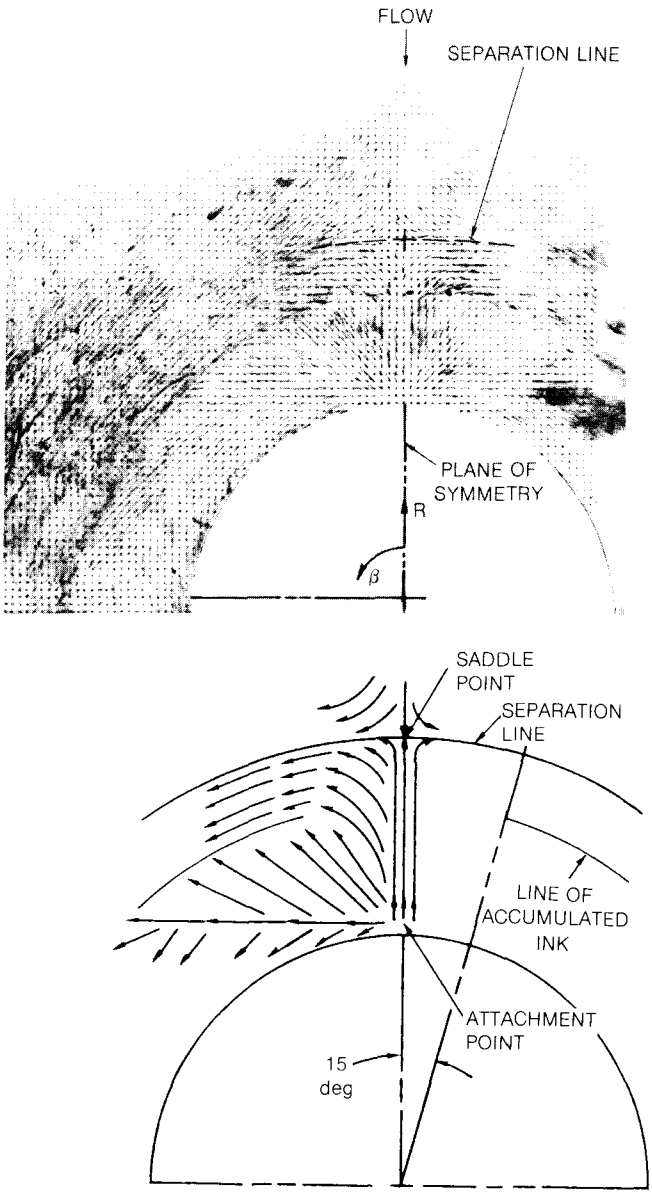

FIG. 13 ENDWALL FLOW VISUALIZATION AND FLOW DIAGRAM

symmetry. No other singular points can be identified in this plane as all streaklines between these two points indicate flow away from the attachment point toward the saddle point. The dashed line indicates the separation line corresponding to the saddle point. This endwall pattern is indicative of a single horseshoe vortex, as was measured with the five-hole probe.

The five-hole probe data show that the horesehoe vortex was formed between the plane of symmetry and the 25-deg plane. The endwall flow visualization indicates that the flow adjacent to the endwall rolled up into the vortex at approximately β = 15 deg. The streak pattern between the plane of symmetry and β = 15 deg indicates that reverse flow moved toward the separation line and then proceeded tangentially around the cylinder. Beyond the 15-deg plane, reverse flow streaklines abruptly stop where a line of accumulated ink can be seen. This pattern indicates that reverse flow adjacent to the endwall rolled up into the fluid interior beginning in the vicinity of the 15-deg plane. The line of accumulated ink can be interpreted as a separation line. The flow visualization clearly shows, however, that this separation line does not extend from a second saddle point in the plane of symmetry. In the terminology of Tobak and Peake [10], then, this line of accumulated ink represents a local separation line.

DISCUSSION

The vortex pattern deduced from the experimental data is shown in Fig. 14. Near the plane of symmetry, low-loss fluid from outside the aproaching boundary layer passed next to the cylinder, stagnated at the endwall-cylinder junction, and proceeded back toward the saddle point adjacent to the endwall. Streamwise flow in the boundary layer followed the same pattern but turned inside of the low-loss fluid. The interaction between reverse flow and incoming flow, which separated at a shallow angle, led to the reverse flow accerating away from the cylinder. Incoming flow eventually blocked reverse flow, forcing the reverse flow to deccelerate. Rather than rolling up into a vortex, the low momentum flow tended to turn and pass tangentially around the cylinder adjacent to the separation lines. Reverse flow away from the plane of symmetry followed the same pattern, but turned at radial locations closer to the cylinder as reverse flow from closer to the plane of symmetry occupied the region next to the separation line. Eventually this accelerating reverse flow contained too much momentum to adjust to the sharp turning required to pass tangentially around the cylinder. The reverse flow then rolled up into a vortex. The five-hole probe measurements show that the vortex was present in the 25-deg plane but not in the 5-deg plane. The endwall visualization pattern indicates that flow adjacent to the endwall became involved in the vortex beginning at $\beta = 15$ deg.

This flow pattern does not support the multiple vortex pattern given by Baker [8] and Moore and Forlini [11]. That pattern was developed from endwall flow visualizations where the local separation line identified in this experiment was interpreted as a global separation line emanating from a second saddle point in the plane of symmetry. Based on the flow topology, a nodal point of attachment must be present between the two saddle points, though the nodal point could not be discerned in the endwall flow visualizations. Based on these results, the expermientors inferred a multivortex system for the separation of the boundary layer from the endwall. This complex vortex system was not present in this experiment. The endwall flow visualization clearly shows a single saddle point, and the flow field measurements indicate a single horseshoe vortex.

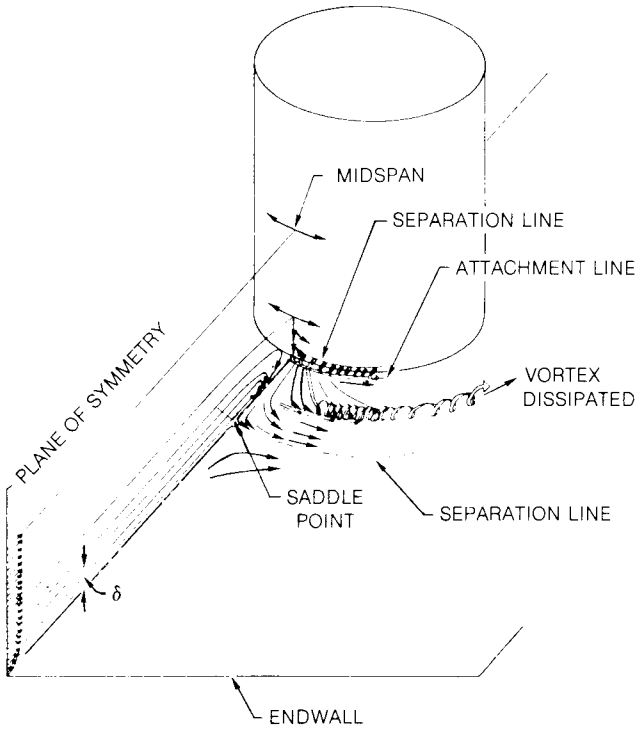

FIG. 14 HORSESHOE VORTEX FORMATION

CONCLUSIONS

This project documented the flow field in the endwall region around a cylinder. This documentation leads to the following conclusions:

1. A single endwall saddle point and a single endwall attachment point were observed in the endwall flow visualization pattern. The multiple singular points required for the multivortex model were not present.
2. The five-hole probe measurements indicate that a single main vortex was formed. Though the rudiments of a vortex were observed in the plane of symmetry and the 5-deg plane, the vortex was fully formed between the 5-deg and 25-deg planes. The flow visualization pattern indicates that the flow adjacent to the endwall initially rolled up near the 15-deg plane.
3. The main vortex was confined to a region less than one boundary-layer thickness from the endwall. The vortex core moved radially outward and slightly away from the endwall as the vortex passed around the cylinder.
4. The losses associated with the vortex rollup were localized and offset by the transport of core flow into the endwall region next to the cylinder.
5. A key implication of these experimental results for gas turbine engines is that flow in the saddle point region does not exhibit swirl.

ACKNOWLEDGEMENTS

This work was supported by NASA Grant No. NSG-3238 under the direction of L. J. Goldman of the NASA Lewis Research Center.

REFERENCES

1. Eckerle, W. A., "Horseshoe Vortex Formation Around a Cylinder", Ph D. Thesis, University of Connecticut, Storrs, Connecticut, May, 1985.
2. Langston, L. S., Nice, M. L. and Hooper, R. M., "Three Dimensional Flow Within a Turbine Cascade Passage", Trans. ASME, Journal of Engineering for Power, Vol. 99, January, 1977, pp. 21-28.
3. Langston, L. S. and Boyle, M. T., "A New Surface-Streamline Flow-Visualization Technique", Journal of Fluid Mechanics, Vol. 125, pp. 53-57, 1982.
4. Langston, L. S. and Wagner, C. A., "A Streamline Model for a Saddle Point of Separation", Submitted to the Journal of Fluid Mechanics, October, 1983.
5. Oswatitsch, K., "Die Ablosungsbedingung von Grenzchichten", Symposium on Boundary Layer Research, International Union of Theoretical and Applied Mechanics, Edited by Gortler, Springer Verlay, Berlin, 1958.
6. Ram, V. V., "Untersuchungen uber die Eckengrenzschicht an einem Kreiszylinder mit Seitenwand", Report 63/46, Institute of Fluid Mechanics, Technische Hochschule, Braunschweig, 1963.
7. East, L. F. and Hoxey, R. P., "Low Speed Three-Dimensional Turbulent Boundary Layer Data", Royal Aircraft Establishment, Tech. Rep. No. 69041, Parts I and II, 1969.
8. Baker, C. J., "Vortex Flow Around the Bases of Obstacles", Ph. D. Thesis, University of Cambridge, Cambridge, England, September, 1978.
9. Schlichting, H., Boundary Layer Theory, McGraw-Hill, 1968, 596-651.
10. Tobak, M. and Peake, D. J., "Topology of Three-Dimensional Separated Flows", Ann. Rev. Fluid Mechanics, Vol. 14, pp. 61-85, 1982.
11. Moore, J., and Forlini, T. J., "A Horseshoe Vortex in a Duct", Trans. of the ASME, Journal of Engineering for Gas Turbines and Power, Vol. 106, July 1984, pp. 668-676.